

SCIENTIFIC REPORTS



OPEN

Facile and inexpensive fabrication of zinc oxide based bio-surfaces for C-reactive protein detection

Lu Cao, Janice Kiely, Martina Piano & Richard Luxton

The paper reports a biosensor formed from antibody coated ZnO nano-crystals which has been prepared using a rapid and inexpensive fabrication method which utilises colloidal dispersion enhanced using sonication. This technique was used to prepare highly ordered and uniform nano-crystalline sensor surfaces on polyethylene terephthalate (PET) using 0.5%, 1% and 5% concentrations of zinc oxide nano-crystal suspensions. Impedance spectroscopy was employed to interrogate the sensor surfaces and confirmed high reproducibility of the fabrication process. Changes in impedance values, at a frequency of 138 Hz, were used to establish dose dependent responses for C-reactive protein (CRP) antigen. A limit of detection of less than 1 ng/ml was demonstrated for nano-surfaces fabricated from concentrations of 1% ZnO.

Nanomaterials have been intensively studied and provide an excellent platform for the development of high performance biosensors, due to their unique physio-chemical properties. For example, due to the large surface area of nanomaterials, large numbers of capture molecules, such as enzymes¹⁻³, antibodies⁴, and DNA⁵, can be immobilised, enhancing sensitivity. Zinc oxide (ZnO) nanoparticles are one of the most important nanomaterials in this context, due to their high electron mobility, good chemical stability, low toxicity and biological compatibility⁶. Furthermore, ZnO has a high isoelectric point (pI) of approximately 9.5, which makes it suitable for absorption of relatively negatively charged proteins, e.g. enzymes and antibodies with lower pI's, primarily driven by electrostatic interaction. The majority of reported ZnO-based biosensors are designed for the detection of various molecule analytes by electron transfer, such as glucose^{3,7,8}, cholesterol^{9,10}, cortisol¹¹, cardiac troponin (cTnT)¹² and phenol¹³. It has been used for detection of pentachlorophenol (PCP) via measuring electrochemiluminescence (ECL) intensity at electrode surface caused by electrochemical high-energy electron transfer reaction¹⁴. ZnO also has been used to fabricate electrochemical impedance spectroscopy (EIS) based sensors for detection of glucose⁸. Furthermore, EIS has also been shown to indicate the effect of different cTnT concentrations on the charge perturbations at the electrode surfaces¹².

From a structural perspective, zinc oxide crystallizes in two main forms, hexagonal wurtzite and cubic zinc blende, the wurtzite structure is most stable at ambient conditions and thus most common. ZnO can produce a piezoelectric effect once it is strained due to the non-centrosymmetric crystal structure¹⁵. The piezoelectric constant is strongly sensitive to both temperature and stress¹⁶. Because of the role of native point defects and impurities, innately ZnO has an n-type conductivity¹⁷. A number of methods have been used to synthesize ZnO films and other types of nanostructures for biosensors, such as chemical baths¹⁸, hydrothermal methods¹⁹, chemical vapour deposition (CVD)²⁰, Pulsed Laser Deposition (PLD)¹¹, sputtering²¹, electro-spinning² and sweeping-printing²². However, the preparation of these films and structures, such as nanowires¹⁸, nanorods^{4,9,21}, nanofibres² and nanotubes^{1,23}, with desirable electrical/chemical properties remains a technological challenge. One example of the complexity of achieving high quality, reproducible structures is described by Sanguino²⁴. They used hydrothermal process to gain a high density of ZnO structures deposited on Au microelectrodes, however, the lack of deposition time caused the uneven coverage of the electrode²⁴.

Compared with other methods, the technique of colloidal dispersion of ZnO nanoparticles shows both disadvantages and advantages. The disadvantage of ZnO nano-crystals is that the crystals easily aggregate. During the process of growth, Park *et al.*²⁵ found that several ZnO crystallites of about 5–10 nm agglomerated and formed a horizontal hexagonal platelet, which was a different output compared with other published results. Through a comparison of different concentrations (1%, 3%, 5% and 7%) of ZnO dispersions either in water or methanol to make the surface of ZnO-polyester composite textile materials, Rimbu *et al.*²⁶ demonstrated that the larger

Institution of Bio-sensing Technology, University of the West of England, Frenchay Campus, Bristol, BS16 1QY, UK. Correspondence and requests for materials should be addressed to L.C. (email: Lu2.Cao@live.uwe.ac.uk)

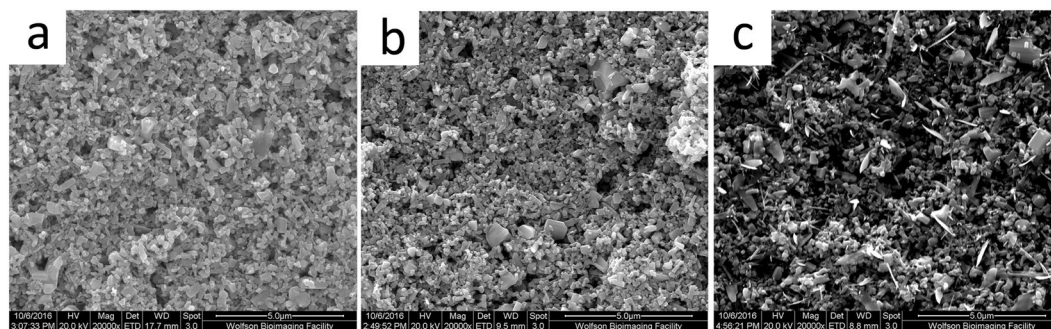


Figure 1. SEM images for ZnO nano-surfaces on PET via suspensions at different amounts of ZnO nano-crystals: (a) 5% ZnO; (b) 1% ZnO; (c) 0.5% ZnO.

concentration leads to agglomerations and a diminished coating quality. In order to mitigate the problem of aggregation, the process of sonication can be used. For example, in order to fabricate an ultrasensitive biosensor for DNA detection, Liu *et al.*⁵ employed sonication to achieve water-soluble ZnO/Au nanocomposites. The advantage of the colloidal dispersion techniques is that ZnO nanocrystals of defined shape and size can be purchased ensuring that well characterised films can be created via a simple fabrication process.

In this study, we present preliminary results of a new biosensor that utilises a colloidal dispersion technique, incorporating sonication, to create a ZnO nanocrystal surface. The advantage of this technique is that biosensor surfaces, with controlled compositions and nanostructures, could be created at low cost with standard laboratory equipment; the technique also being suitable for large scale synthesis. Impedance spectroscopy was used to interrogate the biosensor surface to create a compact biosensor. In order to prove the functionality of the ZnO nano-crystal biosensor, C-reactive protein (CRP) was selected as the model antigen. CRP has been shown as a biomarker of various health outcomes, such as cardiovascular disease²⁷, obesity²⁸, diabetes²⁹, cerebrovascular disease³⁰, chronic kidney disease³¹, cancer³².

Results and Discussion

Morphological Study. From the SEM images, Fig. 1(a), the 5% ZnO suspension shows a surface with a more complete covering of ZnO compared with Fig. 1(b), the 1% ZnO suspension. This observation was as expected owing to the larger mass of ZnO applied. Figure 1(c) shows that the surface of 0.5% ZnO nano-crystals on PET is significantly different from the 1% and 5%, with abnormal sharp, platelet-like shapes. We postulate that the relative absorption of ultrasound energy is greater by the crystals when there is a lower mass of ZnO material (0.5% ZnO), resulting in the fracture of the ZnO crystals forming the observed sharp platelets. This suggests that the size of the composites observed could be due to the sonication-induced aggregation⁵. In other words, the lower concentrations of ZnO suspension are subject to larger shear forces which may fracture the existing nanocrystal structures and subsequent agglomerations result in the formation of the other ZnO nano-structures observed.

From Fig. 2 it is clear that even though the surface is covered with dense nanoparticles, there are still many voids resulting in a porous surface. The lower values of grayscale represent darker areas on the image where the substrate is revealed and the higher grayscale values represent the lighter areas with a maximum grayscale value of 255. The profile plot of 5% ZnO shows the narrowest range of grayscale values compared with 1% and 0.5%, indicating that the surface of 5% is smoother than the others, with less deep holes and peaks across the nano-surface, reflecting the high density of ZnO nanocrystals present. This demonstrates that the colloidal dispersion technique and drop method provides uniformed ZnO films with 5% ZnO. In comparison, the 1% ZnO nano-surface gave full coverage with ZnO but with a rougher surface, whereas the 0.5% nano-surface showed many areas where the grayscale value was zero, indicating deep pits, revealing the underlying PET. The roughness index of the 0.5% ZnO nano-surface was calculated to be 8097, the 1% ZnO nano-surface was 10718 and the 5% ZnO nano-surface was 2310. These results indicate that 1% ZnO nano-surface has the largest surface area; the 0.5% ZnO nano-surface had a relatively large surface area but there was incomplete coverage of the PET substrate, whereas the 5% nano-surface is the least rough, with the smallest surface area.

Raman Spectroscopy analysis of the surfaces. Figure 3 shows the Raman spectra of bare PET (blue line) and PET covered with 1% ZnO nanocrystals (green line). There was a strong correlation with a Raman spectrum of pure PET³³, two strong, characteristic bands were observed at 1723 cm^{-1} and 1610 cm^{-1} which corresponded to C=O stretching and benzene ring structures. The band at 854 cm^{-1} corresponded to the ester C(O)O bending mode³³. Published Raman spectra of ZnO nanorods^{34,35}, indicate significant bands at 438 cm^{-1} and 1050 cm^{-1} and a few weak bands at 330, 379, 535 and 585 cm^{-1} . The Raman spectrum of the ZnO surface shown in Fig. 3, shows that the bands associated with the PET are attenuated due to being covered by ZnO, additional bands are seen at 324, 435, 532, 582 and 1050 with the significant bands at 324 cm^{-1} and 1050 cm^{-1} . These results strongly indicate the ZnO nano crystals cover the surface. A Raman peak at 324 cm^{-1} represents a highly crystalline structure in ZnO nanomaterials, while peaks at 584 and 673 cm^{-1} represent disordered material and impurities³⁶. Comparing the intensity of two peaks at 324 and 582 cm^{-1} , the peak at 324 cm^{-1} was far greater, indicating that the nano-surface with ZnO crystals were highly ordered and uniform.

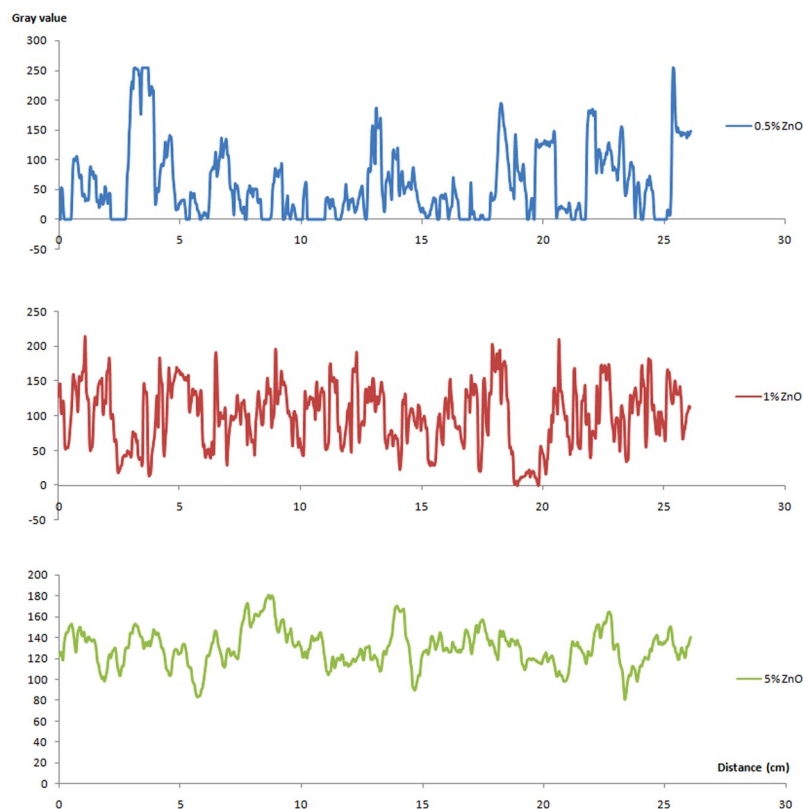


Figure 2. Plot profiles along a horizontal line within images (mag \times 2000) for nano-surfaces made by three different concentrations of ZnO suspensions: 0.5%, 1% and 5%.

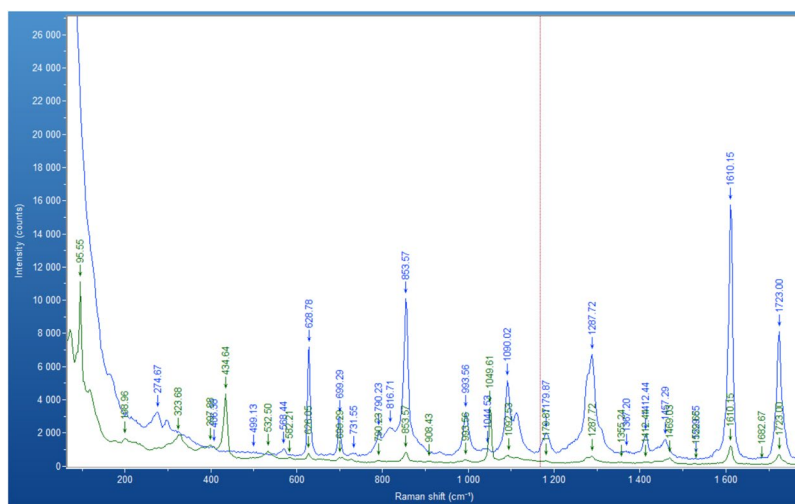


Figure 3. Raman spectra of bare PET (blue line) and PET covered by 1% ZnO nanocrystals (green line) at room temperature. Conditions of recording Raman Spectrum of bare PET: time acquisition 30 s, wavelength 785 nm. Conditions of recording Raman Spectrum of nano-ZnO on PET: time acquisition 50 s, wavelength 785 nm.

Figure 4 shows the Raman spectra for 1% ZnO with capture antibody (green line) and for ZnO without the capture antibody molecule (blue line). The main goal is to identify antibody on the surface of the ZnO through the spectra derived. The anti-Human C-reactive protein, used in this study is an IgG2a isotype. Bands associated with antibody were observed at 2937, 2576, 2211, 1125, 999 and 914 cm^{-1} , providing strong evidence that antibody is on the surface of the ZnO nanocrystals. Kengne-Momo³⁷ reports that IgG will give bands at 914 cm^{-1} (CH_2 deformation (ρCH_2)); 2937 cm^{-1} (C-H stretching ($\nu\text{C-H}$) of aliphatic chains). Both of these bands are evident in Fig. 4. In addition, the backbone skeletal $\nu\text{C-C}$ vibration bands were observed in the region of 999 to 1125 cm^{-1} .

Different concentrations of ZnO suspensions dropped on PET	N	Mean	StDev	CV(%)
5%	24	352870	2453	0.70
1%	24	345567	4117	1.19
0.5%	24	338387	5633	1.66

Table 1. Data analysis on impedance values on each set of ZnO nano-surfaces at fixed frequency.

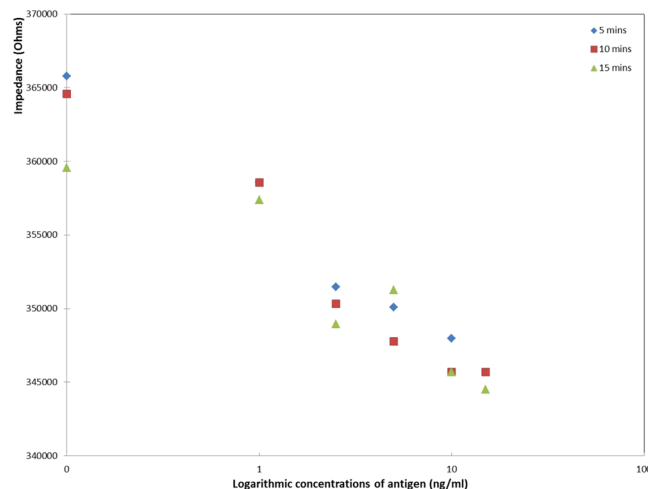


Figure 6. Impedance values from 1% ZnO nano-sensors, with 100 ng capture antibody with increasing concentrations of antigen: 0–15 ng/ml, for 5, 10 and 15 minutes incubation time.

a logarithmic function of CRP concentration for each of the 3 nano-surfaces. The plots were similar indicating that beyond 5 minutes the incubation time does not greatly influence the result, which suggests that binding of CRP to the antibody occurs rapidly. The dose dependent response of absolute impedance for each incubation time shows decreasing impedance with increasing CRP loading. This can be explained by the fact that in this experimental set-up the ZnO is positively charge, whereas the CRP is dominated by negative charge (pI of CRP is ~ 5.45). Electrochemical impedance spectroscopy (EIS) can be used to measured an electrical double layer (EDL) formed when a semiconducting material interacts with liquid electrolytes¹¹. Consequently, when binding to the ZnO occurs, through capture by the antibody on the surface, there is a decrease in the overall positive charge with increasing CRP loading and a decrease in the absolute impedance value. This observation concurs with the literature where it is reported that, for non-faradaic biosensors, changes in the surface dielectric and charge distribution are induced when a protein target binds to the receptor, previously attached in the electrode, displacing water and ions from the surface³⁹.

The nano-surfaces fabricated from different ZnO suspensions were compared by measuring impedance changes with 100 ng capture antibody by adding different concentrations of CRP from 0 to 15 ng/ml at 138 Hz with 10 minutes incubation time. These experimental conditions were selected because, as described above, reproducible differences between the samples were evident at 138 Hz. In addition, from Fig. 6, the absolute impedance measurement have shown to perform reliably with a 10 minutes incubation time. The modulus of the impedance differences (impedance value minus the blank) were employed to plot a calibration curve as shown in Fig. 7. The impedance difference plot shows increasing values of the modulus of the impedance difference with increasing concentrations of CRP for 0.5% and 1% ZnO nano-surfaces. A dose dependence relationship is shown for each plot and can be explained as for Fig. 6 (the opposite slope relating to the fact that Fig. 7 is the modulus of the difference, whereas Fig. 6 shows absolute impedance measurement).

EIS has been shown to be effective tool for probing the interfacial properties such as the charge transfer and charge separation⁷. Figure 7 shows that biosensors prepared with 1% ZnO gave higher output for each concentration of CRP compared with 0.5%. The performance of the biosensors is related to the availability of antibody on the surface to bind CRP. Increasing concentrations of antigen binds to a fixed amount of antibody in a dose dependent manner defined by the binding affinity. We speculate that there is increased charge accumulation due to the bound antigen on the surface compared with the antigen in solution. In addition, there will be an increased amount of isolated antigen flowing freely in solution, resulting in a decrease in the charge carriers and hence resistance of the solution. Surfaces fabricated using 1% ZnO showed the highest roughness index implying it has the greatest surface area on which the anti-CRP antibody are captured. The low sensitivity of 0.5% ZnO nano-surface is likely to be due to the fact that using 0.5% ZnO the PET surface is not fully covered and that the ZnO exists as “islands” of nanocrystals in a modified form due to the ultrasonication. Because of the thickness of the flatter 5% ZnO nano-surface, it was easy to break during the process of protein immobilization. Consequently, the impedance tests were unstable with big error bars and are excluded in Fig. 7.

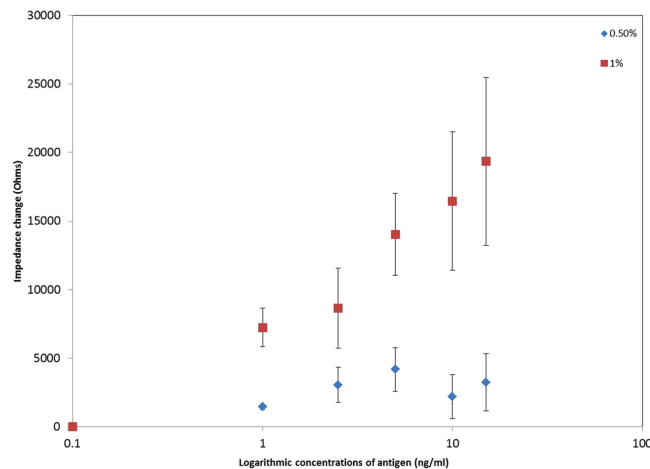


Figure 7. Impedance change in response to increasing concentrations of antigen on 0.5% and 1% ZnO nano-surfaces with 100 ng capture antibody ($n = 3$).

From Fig. 7, it is evident that the limit of detection for 1% is better than 1 ng/ml. (Further work beyond this study is needed to optimise the biosensors and define the specific limit of detection value in each case.) In human blood the normal level of CRP is defined as being less than 10 mg/L which can rise to over 1000 mg/L in cases of severe bacterial infections. Recently the use of high sensitivity measurements of CRP has been shown to be valuable in determining risk of cardiovascular disease. A high sensitivity CRP test (hsCRP) can measure CRP at concentrations of 0.04 mg/L and levels of hsCRP greater than 3.0 mg/L (in the absence of inflammatory processes) is indicative of a high risk of developing cardiovascular disease. The biosensor described in this paper can measure down to 0.001 mg/L and has plenty of scope to allow for dilution of a small blood sample for presentation to a sensor surface and still be able to measure the small changes in CRP concentration related to risk of cardiovascular disease. The biosensor described has the potential to be developed into a rapid, inexpensive diagnostic test for CRP.

Conclusion

Zinc oxide nano-surfaces can be created simply and at low cost using a new colloidal dispersion technique, incorporating sonication. Raman spectra of the surface indicated the ZnO crystal surfaces was highly ordered and uniform. Impedance analysis confirmed that the ZnO surfaces were highly reproducible, individual measurements being taken across many days. SEM analysis illustrated differences in the surfaces when three different ZnO suspension concentrations were applied. The highest concentration studied (5% ZnO) showed the smoothest surface whereas the lowest concentration (0.5%) showed incomplete coverage of the substrate. 1% ZnO demonstrated full coverage of the surface and the largest surface area which was quantified by a roughness index. After addition of the antibody to the ZnO surface, Raman spectroscopy confirmed that there was coverage of ZnO surface with the IgG antibody.

At a fixed frequency of 138 Hz, a dose dependent response was observed from 0.1 ng/ml to 15 ng/ml CRP for all 3 concentrations of ZnO (5%, 1% and 0.5%). A limit of detection of less than 1 ng/ml was indicated for concentrations of 1%. 1% ZnO nano-surface showed the best results with the highest sensitivity. This may be explained by the fact that the 1% ZnO nano-surface has the highest roughness index of the 3 concentrations, calculated from Fig. 2, and hence the largest surface area for binding. In contrast, the 0.5% ZnO nano-surface shows incomplete coverage, high variability of particle size and shape and also the lowest sensitivity. Interestingly, during biosensor preparation, the 1% ZnO nano-surface was more stable than 5% during the process of protein immobilisation. The method for fabrication of ZnO nano-surface via colloidal dispersion coupled with ultra-sonication is simple and inexpensive and we consider that this is a promising area for future research. Further work is required to fully characterise the biosensor and to optimise the process of fabricating nano-surface and protein immobilisation to confirm the excellent reproducibility.

Methods

Materials. Zinc oxide nanopowders (ZnO, 99.9 + %, 80–200 nm) were purchased from US Research Nanomaterials Inc. Biological molecules: monoclonal mouse anti-human C-reactive protein (4C28 Mab: C6) and human C-reactive protein (CRP) (8C72) were purchased from HyTest Ltd. Phosphate Buffered Saline (PBS, pH 7.3 ± 0.2 at 25 °C) was purchased from OXOID Microbiology products. The PBS buffer was diluted to 0.025 M adjusting the pH to 7.4.

Surface preparation. Accurately weighed quantities of ZnO nano-crystals were added to double deionized water to make a range of concentrations of ZnO suspensions: 0.5%, 1% and 5%. The ZnO suspensions were stirred for one hour and then 1.5 ml aliquots were ultra-sonicated for 7 periods of 20 seconds, at 4 minutes intervals using an exponential microprobe (Soniprep 150) at 30 watts. 200 μ l ZnO suspensions were dropped onto

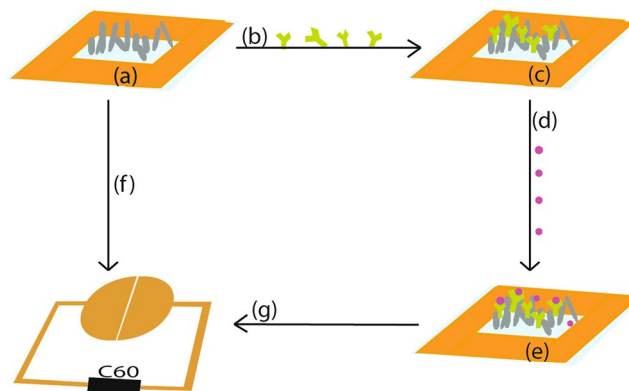


Figure 8. Schematic illustration of biosensor fabrication and sensing: The ZnO sensing area was defined using tape (a); then the antibody was added to the ZnO surface (b) and dried at 4 °C overnight (c); different concentrations of CRP were prepared (d) and added to the immobilised antibody on the ZnO surface (e); the impedance was measured on a blank surface (f) and a surface subjected to the assay protocol (g).

clean polyethylene terephthalate (PET) surface. Subsequently, they were dried in oven at 65 °C for 80 minutes and cooled to room temperature and stored in a dry atmosphere with silica gel for up to 2 days.

CRP Sensor fabrication and test. The sensing area (10 × 4 mm) of ZnO nanoparticles was defined by tapes (Fig. 8a). Subsequently, 40 μl (100 ng) antibody (C6) was added to the surface (Fig. 8b). The biosensor was then dried in a desiccator with silica gel at 4 °C overnight for 18 hours (Fig. 8c) without wash.

A Cypher Instruments C60 Impedance-Amplitude-Phase Analyser was used to measure the impedance of the nano-crystal surfaces (Fig. 8f). The frequency was scanned from 10 Hz to 4 MHz at a voltage of 2 V_{pp}, and a DC offset of 0.9 mV, with 300 test points. The impedance plots were analysed using Cypher Graph V1.21.0, Impedance Amplitude and Phase Analyser graphing application software. Impedance spectra of ZnO nano-surfaces were acquired on 24 independent measurements at each of the three concentrations of ZnO used to prepare the surface.

Statistical tests were performed using Minitab. The %CV = (Standard Deviation/Mean*100) was used to compare variation and demonstrate reproducibility within groups. A 2-Sample t-test for between group comparisons was used to prove significant differences, a p value of <0.05 was considered significant.

CRP was prepared at a range of concentrations: 0 (PBS only), 1, 2.5, 5, 10, and 15 ng/ml in PBS (Fig. 8d). 75 μl of each concentration of antigen was added to the biosensor (Fig. 8e) without wash. Following set incubation times the impedance was measured (Fig. 8g) without wash. Impedance measurements were also made at each stage of the assay process, namely: (1) On the nano-crystal surfaces with dry antibody; (2) Instantly, after adding 75 μl of different concentrations of antigen and (3) at 5 minutes intervals until 30 minutes incubation time had passed. In order to plot logarithmic concentrations of CRP, the measurement of PBS buffer only with no CRP (the blank), was defined 0.1 ng/ml CRP (rather than 0 ng/ml). The difference in impedance was derived by subtracting the blank impedance value from each impedance measurement of the CRP assay at the various concentrations.

Characterization. The morphology of ZnO nano-surface was analysed by Scanning Electron Microscopy (SEM). The samples were coated with a thin layer of Au prior to analysis. A grayscale profile of each image was created using Image J software. Grayscale values along a horizontal line comprising 966 points, were used to produce a 'Roughness Index'. A grayscale value (0–255) is a single number that represents the brightness of the pixel. The light areas indicate charge on the surface in the SEM with higher points reflecting electrons and accumulating charge more easily. This means that “deeper” areas do not reflect or accumulate charge as readily and consequently have lower values. Roughness Index was defined as the summation of absolute changes in grayscale values between each two adjacent points. Consequently, the Roughness Index gives an indication of surface area; a larger index means a larger surface area. Grayscale value plots were derived from the images shown in Fig. 1(a,b,c) by placing a horizontal line across the image using ImageJ software, as shown in Fig. 2.

Raman spectroscopy was used to distinguish the chemical compositions of the ZnO nano-crystal surfaces. A XploRA Raman spectrometer from Horiba, equipped with a confocal microscope, was used. The Raman signals were collected in a range of 0–3500 cm⁻¹ using a 785 nm red laser excitation. The laser beam was focused on the sample using objective magnification of 50×.

References

1. Yang, K. *et al.* ZnO Nanotube Arrays as Biosensors for Glucose. *J. Phys. Chem. C* **113**, 20169–20172, <https://doi.org/10.1021/Jp901894j> (2009).
2. Zhao, M. G. *et al.* The application of porous ZnO 3D framework to assemble enzyme for rapid and ultrahigh sensitive biosensors. *Ceram. Int.* **39**, 9319–9323, http://ac.els-cdn.com/S0272884213005580/1-s2.0-S0272884213005580-main.pdf?_tid=0954e584-baa1-11e4-b634-00000aab0f02acdnat=1424616333_16ab3ec86f0ac034a67f9237e2e063f5, <https://doi.org/10.1016/j.ceramint.2013.05.047> (2013).
3. Jung, J. & Lim, S. ZnO nanowire-based glucose biosensors with different coupling agents. *Appl. Sur. Sci.* **265**, 24–29, http://ac.els-cdn.com/S0169433212017941/1-s2.0-S0169433212017941-main.pdf?_tid=1091df8c-baa1-11e4-91ad-00000aacb35facdnat=1424616345_63b8cc087d2085804707b6964dcf7138, <https://doi.org/10.1016/j.apsusc.2012.10.069> (2013).

4. Shen, Y. C. *et al.* IGZO thin film transistor biosensors functionalized with ZnO nanorods and antibodies. *Biosens Bioelectron* **54**, 306–310, http://ac.els-cdn.com/S0956566313007458/1-s2.0-S0956566313007458-main.pdf?_tid=17d3bae0-baa1-11e4-8115-00000aacb35dacdnat=1424616358_888e6c2cbb6f48d6045c084c7433ef, <https://doi.org/10.1016/j.bios.2013.10.043> (2014).
5. Liu, Y. *et al.* Biocompatible ZnO/Au nanocomposites for ultrasensitive DNA detection using resonance Raman scattering. *J Phys. Chem. B* **112**, 6484–6489, <http://www.ncbi.nlm.nih.gov/pubmed/18444675>, <https://doi.org/10.1021/jp710399d> (2008).
6. Wang, Z. L. Towards self-powered nanosystems: From nanogenerators to nanopiezotronics. *Adv. Funct. Mater.* **18**, 3553–3567, <https://doi.org/10.1002/adfm.200800541> (2008).
7. Anusha, J. R. *et al.* Simple fabrication of ZnO/Pt/chitosan electrode for enzymatic glucose biosensor. *Sensors and Actuators B-Chemical* **202**, 827–833, http://ac.els-cdn.com/S0925400514007138/1-s2.0-S0925400514007138-main.pdf?_tid=5c38ef14-c255-11e4-b884-00000aacb361acdnat=1425463440_babfee9bf8c2c24f0da9ed1e61ed19d9, <https://doi.org/10.1016/j.snb.2014.06.024> (2014).
8. Munje, R. D., Muthukumar, S. & Prasad, S. Lancet-free and label-free diagnostics of glucose in sweat using Zinc Oxide based flexible bioelectronics. *Sensors and Actuators B-Chemical* **238**, 482–490, http://ac.els-cdn.com/S0925400516311236/1-s2.0-S0925400516311236-main.pdf?_tid=e9290176-2bfc-11e7-ad7c-00000aab0f27acdnat=1493375270_7c24914094d99418b368d45cf7c6e699, <http://www.sciencedirect.com/science/article/pii/S0925400516311236>, <https://doi.org/10.1016/j.snb.2016.07.088> (2017).
9. Ahmad, R., Tripathy, N. & Hahn, Y. B. Wide linear-range detecting high sensitivity cholesterol biosensors based on aspect-ratio controlled ZnO nanorods grown on silver electrodes. *Sensors and Actuators B-Chemical* **169**, 382–386, http://ac.els-cdn.com/S0925400512004765/1-s2.0-S0925400512004765-main.pdf?_tid=0dfd8c12-baa1-11e4-9d0b-00000aab0f26acdnat=1424616341_284417d1837192d8d31c3e7c247aace3, <https://doi.org/10.1016/j.snb.2012.05.027> (2012).
10. Batra, N., Tomar, M. & Gupta, V. ZnO–CuO composite matrix based reagentless biosensor for detection of total cholesterol. *Biosens. Bioelectron.* **67**, 263–271, <http://www.sciencedirect.com/science/article/pii/S0956566314006174>, http://ac.els-cdn.com/S0956566314006174/1-s2.0-S0956566314006174-main.pdf?_tid=48df3844-ba79-11e4-b02e-00000aab0f6cacdnat=1424599260_2b83d580a549c4e2d81a03cff28df646 <http://ac.els-cdn.com>, <https://doi.org/10.1016/j.bios.2014.08.029> (2015).
11. Munje, R. D., Muthukumar, S., Selvam, A. P. & Prasad, S. Flexible nanoporous tunable electrical double layer biosensors for sweat diagnostics. *Sci. Reports* **5**, <https://doi.org/10.1038/Srep14586> (2015).
12. Shanmugam, N. R., Muthukumar, S. & Prasad, S. Ultrasensitive and low-volume point-of-care diagnostics on flexible strips - a study with cardiac troponin biomarkers. *Sci. Reports* **6**, <https://doi.org/10.1038/Srep33423> (2016).
13. Gu, B. X. *et al.* Tyrosinase immobilization on ZnO nanorods for phenol detection. *J Phys Chem B* **113**, 377–381, <http://www.ncbi.nlm.nih.gov/pubmed/19067557>, <https://doi.org/10.1021/jp808001c> (2009).
14. Jiang, D. *et al.* One-step thermal-treatment route to fabricate well-dispersed ZnO nanocrystals on nitrogen-doped graphene for enhanced electrochemiluminescence and ultrasensitive detection of pentachlorophenol. *ACS Appl. Mater. Interfaces* **7**, 3093–3100, <http://www.ncbi.nlm.nih.gov/pubmed/25607804>, <https://doi.org/10.1021/am507163z> (2015).
15. Wang, Z. L. From nanogenerators to piezotronics-A decade-long study of ZnO nanostructures. *Mrs. Bull.* **37**, 814–827, <https://doi.org/10.1557/mrs.2012.186> (2012).
16. Ahmad, M., Iqbal, M. A., Kiely, J., Luxton, R. & Jabeen, M. Enhanced output voltage generation via ZnO nanowires (50 nm): Effect of diameter thinning on voltage enhancement. *J. Phys. Chem. Solids* **104**, 281–285, <https://www.sciencedirect.com/science/article/pii/S002236971730032X>, <https://doi.org/10.1016/j.jpcs.2017.01.006> (2017).
17. Janotti, A. & Van de Walle, C. G. Fundamentals of zinc oxide as a semiconductor. *Reports Prog. Phys.* **72**, <https://doi.org/10.1088/0034-4885/72/12/126501> (2009).
18. Sugunan, A., Warad, H. C., Boman, M. & Dutta, J. Zinc oxide nanowires in chemical bath on seeded substrates: Role of hexamine. *J. of Sol-Gel Sci. Technol.* **39**, 49–56, <https://doi.org/10.1007/s10971-006-6969-y> (2006).
19. Ye, N. & Chen, C. C. Investigation of ZnO nanorods synthesized by a solvothermal method, using Al-doped ZnO seed films. *Opt. Mater.* **34**, 753–756, http://ac.els-cdn.com/S0925346711005064/1-s2.0-S0925346711005064-main.pdf?_tid=d6af2584-f184-11e4-9bc3-00000aab0f02acdnat=1430651536_b433781585aac0b51f7515ac0bde02a2, <https://doi.org/10.1016/j.optmat.2011.10.013> (2012).
20. Zheng, X. *et al.* Tunable channel width of a UV-gate field effect transistor based on ZnO micro-nano wire. *Rsc. Adv.* **4**, 18378–18381, <http://pubs.rsc.org/en/content/articlepdf/2014/ra/c4ra01661k>, <https://doi.org/10.1039/C4ra01661k> (2014).
21. Chang, C. J. *et al.* A large area bimaterial sheet of piezoelectric nanogenerators for energy harvesting: Effect of RF sputtering on ZnO nanorod. *Microelectron. Eng.* **88**, 2236–2241, http://ac.els-cdn.com/S0167931710004880/1-s2.0-S0167931710004880-main.pdf?_tid=dc02a164-f184-11e4-9982-00000aab0f6cacdnat=1430651545_57f9b9605f593c324120f57ad93452b, <https://doi.org/10.1016/j.mee.2010.12.010> (2011).
22. Zhu, G. A., Yang, R. S., Wang, S. H. & Wang, Z. L. Flexible High-Output Nanogenerator Based on Lateral ZnO Nanowire Array. *Nano Lett.* **10**, 3151–3155, <https://doi.org/10.1021/Nl101973h> (2010).
23. Roza, L., Rahman, M. Y. A., Umar, A. A. & Salleh, M. M. Direct growth of oriented ZnO nanotubes by self-selective etching at lower temperature for photo-electrochemical (PEC) solar cell application. *J. Alloy. Compd.* **618**, 153–158, <http://www.sciencedirect.com/science/article/pii/S0925838814019689>, <https://doi.org/10.1016/j.jallcom.2014.08.113> (2015).
24. Sanguino, P. *et al.* ZnO nanorods as immobilization layers for interdigitated capacitive immunosensors. *Sensors and Actuators B-Chemical* **204**, 211–217, http://ac.els-cdn.com/S0925400514009083/1-s2.0-S0925400514009083-main.pdf?_tid=39b617fa-2bfd-11e7-a777-00000aacb35eacdnat=1493375405_2f168580de769c82860ffc3a2110d95a, <https://doi.org/10.1016/j.snb.2014.06.141> (2014).
25. Park, H. Y. *et al.* Protective antigen detection using horizontally stacked hexagonal ZnO platelets. *Anal. Chem.* **81**, 4280–4284, <http://www.ncbi.nlm.nih.gov/pubmed/19400578>, <https://doi.org/10.1021/ac900632n> (2009).
26. Rimbui, C. *et al.* Zinc oxide application in the textile industry: surface tailoring and water barrier attributes as parameters with direct implication in comfort performance. *Textile Res. J.* **83**, 2142–2151, <https://doi.org/10.1177/0040517513478460> (2013).
27. Lin, K. C. *et al.* Biogenic nanoporous silica-based sensor for enhanced electrochemical detection of cardiovascular biomarkers proteins. *Biosens. Bioelectron.* **25**, 2336–2342, <https://doi.org/10.1016/j.bios.2010.03.032> (2010).
28. Hsu, L. A. *et al.* Effect of obesity on the association between common variations in the HNF1A gene region and C-reactive protein level in Taiwanese. *Clin. Chimica Acta* **412**, 725–729, <https://doi.org/10.1016/j.cca.2010.12.027> (2011).
29. Rosenson, R. S., Fraser, H., Goulder, M. A. & Hislop, C. Anti-Inflammatory Effects of Varespladib Methyl in Diabetic Patients with Acute Coronary Syndrome. *Cardiovasc. Drugs Ther.* **25**, 539–544, <https://doi.org/10.1007/s10557-011-6344-2> (2011).
30. Kim, S. J., Choe, Y. H., Bang, O. Y. & Collaborators, C.-B. Are Stroke Biomarkers Seeing Brain Vessels in Patients With Ischemic Stroke? A C-Reactive Protein and Homocysteine Study. *Stroke* **42**, 1464–1468, <https://doi.org/10.1161/Strokeaha.110.607432> (2011).
31. Shankar, A. *et al.* Markers of inflammation predict the long-term risk of developing chronic kidney disease: a population-based cohort study. *Kidney Int.* **80**, 1231–1238, <https://doi.org/10.1038/ki.2011.283> (2011).
32. Chaturvedi, A. K. *et al.* C-Reactive Protein and Risk of Lung Cancer. *J. of Clin. Oncol.* **28**, 2719–2726, <https://doi.org/10.1200/Jco.2009.27.0454> (2010).
33. Radoičić, M. B. *et al.* Influence of TiO₂ nanoparticles on formation mechanism of PANI/TiO₂ nanocomposite coating on PET fabric and its structural and electrical properties. *Sur. Coatings Technol.* **278**, 38–47, <http://www.sciencedirect.com/science/article/pii/S0257897215301778>, <https://doi.org/10.1016/j.surfcoat.2015.07.070> (2015).

34. Zhang, R., Yin, P.-G., Wang, N. & Guo, L. Photoluminescence and Raman scattering of ZnO nanorods. *Solid State Sci.* **11**, 865–869, <http://www.sciencedirect.com/science/article/pii/S129325580800335X>, <https://doi.org/10.1016/j.solidstatesciences.2008.10.016> (2009).
35. Zhang, S. *et al.* Hybrid ZnO/ZnS nanoforests as the electrode materials for high performance supercapacitor application. *Dalton Transactions* **44**, 2409–2415, <https://doi.org/10.1039/C4DT03270E> (2015).
36. Umar, A. *et al.* Highly porous ZnO nanosheets self-assembled in rosette-like morphologies for dye-sensitized solar cell application. *New J. Chem.* **39**, 7961–7970, <https://doi.org/10.1039/C5NJ00551E> (2015).
37. Kengne-Momo, R. P. *Protein interactions investigated by the raman spectroscopy for biosensor applications*, vol. 2012 (2012).
38. Jacobs, M., Muthukumar, S., Selvam, A. P., Craven, J. E. & Prasad, S. Ultra-sensitive electrical immunoassay biosensors using nanotextured zinc oxide thin films on printed circuit board platforms. *Biosens. Bioelectron.* **55**, 7–13, <https://doi.org/10.1016/j.bios.2013.11.022> (2014).
39. Santos, A. *Fundamentals and Applications of Impedimetric and Redox Capacitive Biosensors*, vol. S7 (2014).

Author Contributions

R.L. and J.K. conceived the original research idea. L.C. contributed to the research design and carried out the experimentation with help from M.P. L.C. processed the experimental data, all authors discussed the results. L.C. wrote the initial draft of the manuscript, J.K. and R.L. edited the draft and sanctioned the final version of the manuscript.

Additional Information

Competing Interests: The authors declare no competing interests.

Publisher's note: Springer Nature remains neutral with regard to jurisdictional claims in published maps and institutional affiliations.



Open Access This article is licensed under a Creative Commons Attribution 4.0 International License, which permits use, sharing, adaptation, distribution and reproduction in any medium or format, as long as you give appropriate credit to the original author(s) and the source, provide a link to the Creative Commons license, and indicate if changes were made. The images or other third party material in this article are included in the article's Creative Commons license, unless indicated otherwise in a credit line to the material. If material is not included in the article's Creative Commons license and your intended use is not permitted by statutory regulation or exceeds the permitted use, you will need to obtain permission directly from the copyright holder. To view a copy of this license, visit <http://creativecommons.org/licenses/by/4.0/>.

© The Author(s) 2018